Article

Precise Orbit Determination for GNSS Maneuvering Satellite with the Constraint of a Predicted Clock

Xiaolei Dai [1], Yidong Lou [1,*], Zhiqiang Dai [2], Caibo Hu [1,3], Yaquan Peng [1], Jing Qiao [4] and Chuang Shi [1,5]

[1]   GNSS Research Center, Wuhan University, 129 Luoyu Road, Wuhan 430079, China
[2]   School of Electronics and Communication Engineering, Sun Yat-Sen University, No. 135, Xingang Xi Road, Guangzhou 510275, China
[3]   Beijing Satellite Navigation Center, Beijing 100094, China
[4]   Institute of Geodesy and Photogrammetry Geosensors and Engineering Geodesy, ETH Zurich, 8093 Zurich, Switzerland
[5]   School of Electronic and Information Engineering, Beihang University, 37 Xueyuan Road, Beijing 100083, China
*   Correspondence: ydlou@whu.edu.cn; Tel.: +86-027-6877-8595

check for updates

Abstract: Precise orbit products are essential and a prerequisite for global navigation satellite system (GNSS) applications, which, however, are unavailable or unusable when satellites are undertaking maneuvers. We propose a clock-constrained reverse precise point positioning (RPPP) method to generate the rather precise orbits for GNSS maneuvering satellites. In this method, the precise clock estimates generated by the dynamic precise orbit determination (POD) processing before maneuvering are modeled and predicted to the maneuvering periods and they constrain the RPPP POD during maneuvering. The prediction model is developed according to different clock types, of which the 2-h prediction error is 0.31 ns and 1.07 ns for global positioning system (GPS) Rubidium (Rb) and Cesium (Cs) clocks, and 0.45 ns and 0.60 ns for the Beidou navigation satellite system (BDS) geostationary orbit (GEO) and inclined geosynchronous orbit (IGSO)/Median Earth orbit (MEO) satellite clocks, respectively. The performance of this proposed method is first evaluated using the normal observations without maneuvers. Experiment results show that, without clock-constraint, the average root mean square (RMS) of RPPP orbit solutions in the radial, cross-track and along-track directions is 69.3 cm, 5.4 cm and 5.7 cm for GPS satellites and 153.9 cm, 12.8 cm and 10.0 cm for BDS satellites. When the constraint of predicted satellite clocks is introduced, the average RMS is dramatically reduced in the radial direction by a factor of 7–11, with the value of 9.7 cm and 13.4 cm for GPS and BDS satellites. At last, the proposed method is further tested on the actual GPS and BDS maneuver events. The clock-constrained RPPP POD solution is compared to the forward and backward integration orbits of the dynamic POD solution. The resulting orbit differences are less than 20 cm in all three directions for GPS satellite, and less than 30 cm in the radial and cross-track directions and up to 100 cm in the along-track direction for BDS satellites. From the orbit differences, the maneuver start and end time is detected, which reveals that the maneuver duration of GPS satellites is less than 2 min, and the maneuver events last from 22.5 min to 107 min for different BDS satellites.

Keywords: GNSS; precise orbit determination; satellite maneuver; clock prediction; reverse precise point positioning

1. Introduction

A satellite in space tends to drift gradually from its designed orbit because of various perturbations. When the deviation from the designed orbit is larger than the tolerance, the satellite needs to be maneuvered correspondingly to keep its optimal orbit. Two kinds of maneuvers, i.e., in-plane maneuver and out-of-plane maneuver, are usually employed to maintain satellite orbits. An in-plane maneuver is generally implemented by a thrust force in the along-track direction, while the out-of-plane maneuver is applied in the cross-track direction [1,2]. The maneuver frequency depends largely on orbit characteristics, especially the orbit period [3]. The American global positioning system (GPS) consists of 32 Median Earth orbit (MEO) satellites with a revolution period of half a sidereal day. With one satellite of Block III in checkout, there are 31 GPS satellites available (https://www.gps.gov/systems/gps/space/). Each GPS satellite has to be maneuvered about once a year to maintain a regular satellite constellation [4,5]. The Chinese Beidou navigation satellite system (BDS) is rather sophisticated in that it includes five satellites in the geostationary orbit (GEO), five in the inclined geosynchronous orbit (IGSO) and four in the MEO. Xie et al. showed that BDS GEO satellites needed east-west (along-track direction) station-keeping maneuvers every 25–35 days and north-south (cross-track direction) maneuvers about every 2 years [6]. Prange et al. showed that the regular maneuver cycle of BDS IGSO satellites is about half a year [5].

Maneuver may reduce the availability of a global navigation satellite system (GNSS) and degrade the navigation and positioning performance. As early warning information, the approximate repositioning epochs of a maneuvering satellite are published in the notice advisory to navstar users (NANU) message (https://www.navcen.uscg.gov). In addition, this satellite is also flagged as unhealthy in the broadcast ephemeris. However, the published maneuvering epochs are so rough that many normal observations may be discarded. What is more, the unhealthy flags in the broadcast ephemeris are sometimes wrong or missing, which is unreliable and will mislead real-time users [7]. Consequently, some efforts have been made to detect satellite maneuvers. The classical maneuver detection strategy is based on the closest approach of two arcs calculated separately before and after the maneuvering, in which the instantaneous velocity change is determined as the difference between these two arcs at this point [4,8]. This method is adopted by the Center for Orbit Determination in Europe (CODE) to generate the precise orbit products for the International GNSS Services (IGS). Qiao et al. detected BDS satellite maneuvers using the triple-differenced phase residuals from ground monitoring stations [9]. Yan et al. and Ye et al. have used the orbit mutual differences of broadcast ephemeris to detect BDS orbit anomalies and maneuvers [10,11]. Furthermore, Huang et al. proposed a robust maneuver detection method by using the code residuals from reference stations that can be used in real-time [7,12].

In addition to maneuver detection, a maneuver handling operation is necessary to avoid orbit discontinuities or precision degradation during and around maneuvering periods, so that the rather precise orbit products are available. The common approach is introducing pseudo-stochastic parameters to model maneuvers in precise orbit determination (POD), e.g., instantaneous velocity changes at specific maneuvering epochs [13], piecewise constant accelerations over a processing interval [14] or piecewise linear and continuous accelerations at each epoch [15]. These approaches are rather effective to handle maneuvers of satellites in the low Earth orbit (LEO) because of their quick movement and good geometry conditions. Ju et al. showed that the piecewise constant acceleration model contributes to centimeter-level orbit accuracy for the maneuvering LEO satellites [14]. Song et al. and Cao et al. analyzed the performance of different thrust models applied for the maneuvering of BDS GEO satellites and showed that the instantaneous velocity change model results in the best precision of 2–5 m [16,17]. The kinematic POD is an alternative method that is not affected by satellite maneuvers since only observations are employed in this method without any force models. Qiao et al. compared the kinematic and dynamic POD solutions, identified the maneuver thrust force model of BDS satellites and showed that the root mean square (RMS) of the kinematic POD solution with respect to the precise orbit products is less than 0.1 m in the along-track and cross-track directions and larger than 1.0 m in the radial direction [9]. The bad geometry conditions and large position dilution of precision (PDOP)

in the radial direction cause the large orbit error in this direction. Zhou et al. proposed a reverse point positioning (RPP) method using single-frequency code observations to determine the BDS GEO orbits during maneuvers [18]. The orbit accuracy of this method is about 0.92 m, 2.74 m and 8.30 m in the radial, along-track and cross-track directions, respectively, which is a little worse than that of broadcast ephemeris. Considering the strong correlation between clock offsets and the radial component of satellite position, Guo et al. corrected the satellite clock offsets using the measurements of satellite station two-way synchronization (SSTS), bringing improvement to the POD and orbital recovery for the maneuvering BDS satellites. However, the SSTS measurements are not released to the public [19].

Considering that GNSS satellites are generally equipped with atomic clocks that are usually not affected by orbit maneuvers and have high stability and accuracy for short-term prediction [20], we propose a kinematic POD method, the clock-constrained reverse precise point positioning (RPPP), to improve the orbit solutions during maneuvering periods. By constraining the clock offsets with the prediction model, the performance of RPPP during maneuvers can be further improved. This contribution starts with a brief review of maneuver handling in GNSS POD. Next, the clock prediction model and basic mathematics about clock constraining are introduced, based on which the processing scheme of the proposed method is demonstrated. Then, the proposed method is tested on different data sets and the experiment results are analyzed and compared to evaluate the performance of this method. Finally, a summary and conclusions are presented.

2. Methodology

The satellite clock prediction model used in our method is introduced first. Then, we analyze the clock prediction errors and determine the weighting functions during maneuvers for different clock types. At last, the actual processing flow of the clock-constrained RPPP POD strategy for maneuvering satellites is summarized and explained.

2.1. Clock Prediction Model

The stability of a satellite clock can be represented by the factors of phase deviation, frequency deviation and frequency drift. A quadratic polynomic model is usually applied for satellite clock offset prediction which is given as [20,21]

$$c(t) = a_0 + a_1 t + \frac{1}{2} a_2 t^2 + \varepsilon(t) \tag{1}$$

where a_0, a_1 and a_2 are the polynomial coefficients which are corresponding to the clock offset at the initial time, frequency deviation and drift, respectively; $\varepsilon(t)$ is a generic random process noise. Shamliy et al. showed that the quadratic polynomic model is suitable for Rubidium (Rb) clocks, while for Cesium (Cs) clocks, the linear polynomic model is better and the quadratic term a_2 is unnecessary [22]. In addition to linear and quadratic terms, periodic variations should also be added in the prediction model [23]. Pronounced sinusoidal variations are found in GPS satellite clocks and the period equals the orbital period [23]. The clock prediction model with periodic terms can be expressed as [24]

$$\begin{cases} c(t) = a_0 + a_1 t + \frac{1}{2} a_2 t^2 + a_s \sin(\frac{2\pi}{T} t) + a_c \cos(\frac{2\pi}{T} t) + \varepsilon(t), & Rb \\ c(t) = a_0 + a_1 t + a_s \sin(\frac{2\pi}{T} t) + a_c \cos(\frac{2\pi}{T} t) + \varepsilon(t), & Cs \end{cases}$$
$$a_s = A \cos \varphi_0; \quad a_c = A \sin \varphi_0 \tag{2}$$

where A is the amplitude, T is the period of the sinusoid and φ_0 is the corresponding initial phase. When the satellite clock model is identified, the clock model coefficients a_0, a_1, a_2, a_c and a_s can be determined by fitting to the precise clock estimates.

2.2. Constraining of Predicted Clock

In POD of maneuvering satellite, we fit the satellite clock model to the precise clock estimates before maneuvering to determine the model coefficients and then extrapolate the model to the maneuvering and post-maneuvering periods to generate the predicted satellite clocks. The predicted clocks are then introduced as fictitious observations to constrain the satellite clock parameters in the RPPP POD processing, namely
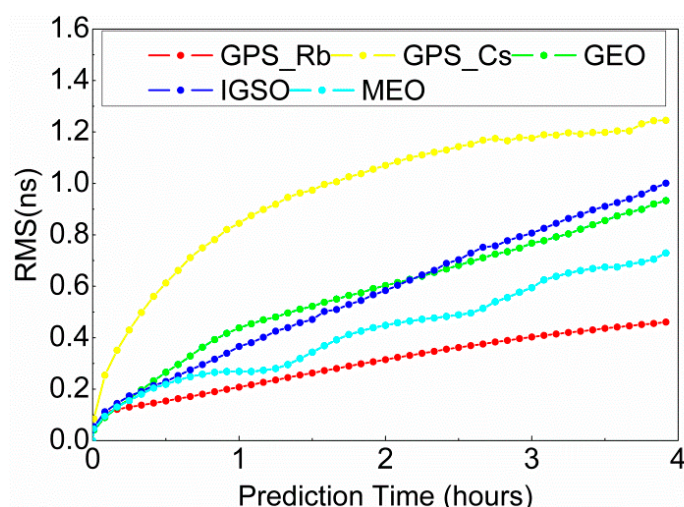
$$\bar{x}_{clk}(t_i) = x_{clk}(t_i) + v(t_i) \tag{3}$$

where $\bar{x}_{clk}(t_i)$ is the predicted clock and $v(t_i)$ is the prediction error at epoch t_i; $x_{clk}(t_i)$ is the satellite clock parameter.

Obviously, the weights of the fictitious observations depend on the prediction error at each epoch. To weight the fictitious observations properly, the precision of the predicted satellite clocks versus prediction time is assessed for GPS and BDS at first. The GFZ 30 s final precise clock products of 2017 are collected and used in this analysis [25]. Specifically, we first fit the clock models to the 24-h clock products to determine the model coefficients in (2) and extrapolate the models to generate predicted clocks for the next 4 h. It is noted that the preprocessing should be carried out to get rid of the large data gaps, outliers as well as the clock jumps [26]. The constant coefficient a_0 is computed with the latest satellite clock estimates in products to avoid possible deviation across the processing boundary [24]. Then, the predicted clocks are compared to the corresponding products, resulting in prediction errors. The RMS of the prediction errors versus prediction time is computed for the GPS Rb, GPS Cs, BDS GEO, BDS IGSO and BDS MEO clocks, the results of which are presented in Figure 1. As shown in this figure, the RMS of prediction errors increases over the prediction time for all clocks. The GPS Rb clocks show the highest prediction accuracy, while that of the GPS Cs clocks is the lowest. The BDS GEO and IGSO satellite clocks exhibit similar precision, which is a little lower than that of the BDS MEO satellites. Then, the weighting function of the fictitious observations can be determined by fitting to the RMS profiles in Figure 1, which is expressed as

$$\gamma(\tau) = \begin{cases} 0.8 \times \sqrt{\tau} & GPS, Rb \\ 0.1 + 0.1 \times \tau & GPS, Cs \\ 0.1 + 0.17 \times \tau & BDS, MEO \\ 0.1 + 0.24 \times \tau & BDS, GEO/IGSO \end{cases} \tag{4}$$
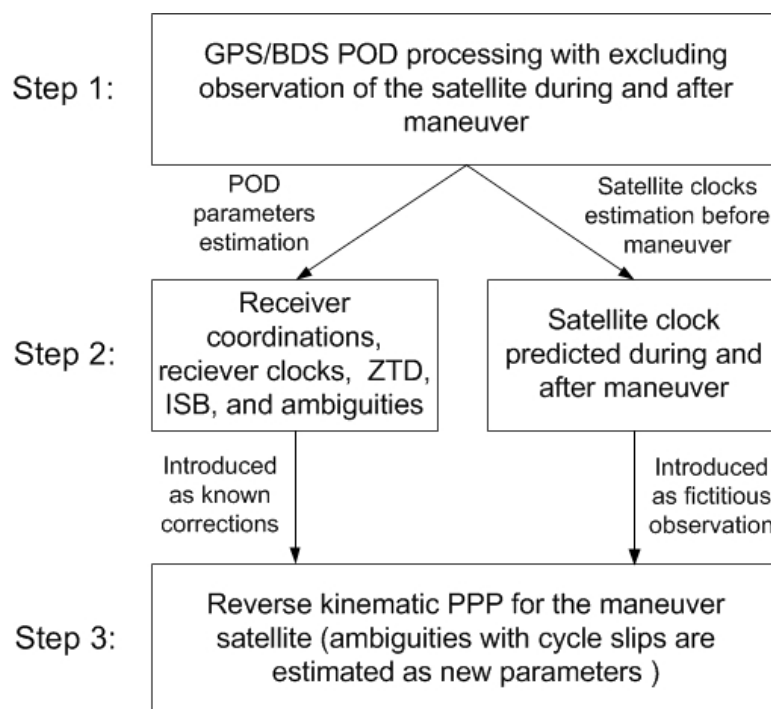
where τ is the prediction time, the unit of which is hours.

Figure 1. Root mean square (RMS) of the prediction errors of different satellite clock types under different time latencies.

2.3. Clock-Constrained Precise Orbit Determination

When the clock prediction model is determined, we can generate predicted clocks to constrain the RPPP during maneuvering. The processing scheme of the clock-constrained RPPP POD strategy for maneuvering satellites is summarized and illustrated in Figure 2. As shown in this figure, the proposed algorithm consists of three steps: the dynamic POD, clock modelling and prediction, and clock-constrained RPPP POD. In step 1, the traditional dynamic POD method is employed to jointly determine the precise orbits of GPS and BDS satellites without the observations of maneuvering satellites during and after the maneuvering. Therefore, the receiver positions, receiver clocks, zenith tropospheric delays (ZTDs), ambiguities and inter-system biases (ISBs) are unaffected by maneuvers and can be precisely determined. In step 2, the clock prediction model for the maneuvering satellites is determined based on the historical clock estimates in step 1. Then, the clock model is extrapolated to the maneuvering and post-maneuvering epochs to generate the predicted clocks. Finally, the RPPP method is employed to determine orbit of the maneuvering satellite based on its observations during and after maneuvering, in which the unknown parameters are fixed, rather than estimated, to the corresponding estimates from step 1 and the predicted clocks are used as fictitious observations to constrain the satellite clock parameters. If there are no cycle slips, the ambiguities of phase observations are corrected for with the latest estimates in step 1. Otherwise, new ambiguity parameters will be introduced and estimated. The weights of the predicted clocks are computed from the weighting function (4). Therefore, only satellite positions, satellite clocks and newly introduced ambiguities need to be estimated in the clock-constrained RPPP processing.
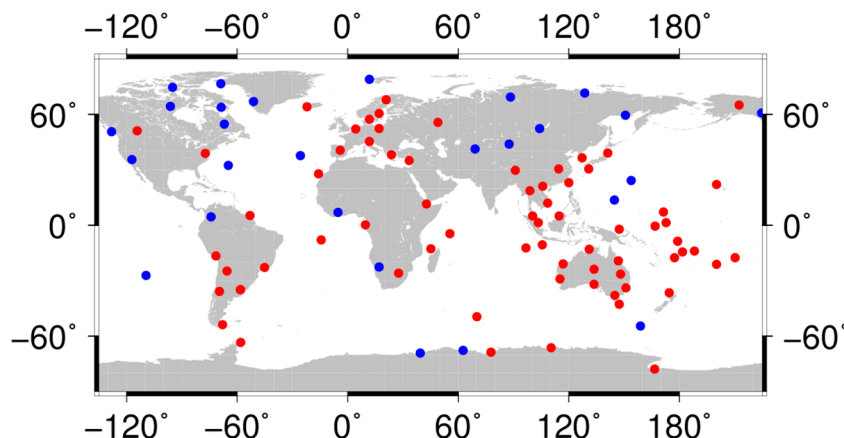

Figure 2. Processing scheme of the clock-constrained reverse precise point positioning (RPPP) precise orbit determination (POD) strategy for maneuvering satellites. GPS—global positioning system; BDS—Beidou navigation satellite system; ZTD—zenith tropospheric delays; ISB—inter-system bias.

3. Experiment Analysis

The proposed method is first evaluated using normal data without maneuvers, since the precise orbit products for satellites during maneuvering are not available. Afterwards, the method is further tested on seven actual maneuver cases, including two GPS maneuver events and five BDS maneuver events.

3.1. Data Collection and Processing Configuration

The experiment data is collected from 25 GPS-only stations of IGS network [27] and 75 GPS + BDS stations of Multi-GNSS Experiment network (MGEX) [28], which are illustrated in Figure 3. The data length is from the day of year (DOY) 121 to 152, 2017, with the sampling interval of 30 s. During this experiment period, two GPS satellites and five BDS GEO satellites experienced orbit maneuvers. The proposed algorithm has been implemented in Positioning and Navigation Data Analyst (PANDA) software for experiment data processing [29,30].

Figure 3. Distribution of stations used in the POD experiment (red: GPS + BDS stations, blue: GPS-only stations).

In POD processing, the code and phase observations on GPS L1/L2 and BDS B1/B2 are used to form the respective ionosphere-free combinations that are processed jointly. The reduced CODE five-parameter solar radiation pressure (SRP) model [31] is applied to all GPS and BDS satellites. For the antenna PCO and PCV of GPS and BDS satellites, we adopted the values provided by IGS. Table 1 lists some of the important configurations of dynamic models and observation models used in the POD experiment.

3.2. Algorithm Validation with Normal Data

It is hard to evaluate the proposed method during maneuvering, because the precise reference orbits are usually unavailable for maneuvering satellites. Therefore, the clock-constrained POD strategy is first evaluated using the normal observations during non-maneuvering periods when the dynamic orbits can be determined precisely and used as a reference in our evaluation. Specifically, the traditional dynamic POD method is employed to determine the 48-h reference orbits for all satellites during the whole experiment periods. Then, we assume a satellite experiences maneuver in the last 2 h of each POD arc when the POD processing is switched from the dynamic method to the RPPP method for the maneuvering satellite. For comparison, the clock constraining function is turned on and off to generate two orbit solutions during the maneuvering periods. The results are both compared to the reference orbits to generate the orbit differences in the along-track, cross-track and radial directions for the last 2 h of each POD arc.

Figure 4 presents the RMS of orbit differences of each satellite in the along-track, cross-track and radial directions for the two RPPP orbit solutions. G04 satellite is excluded in the process because it is flagged as unhealthy for the whole period. As shown in the figure, when the constraints of predicted satellite clocks are not imposed, the average RMS of GPS satellites in the radial, cross-track and along-track directions is 69.3 cm, 5.4 cm and 5.7 cm and that of the BDS satellites is 153.9 cm, 12.8 cm and 10.0 cm, respectively. The GPS satellites exhibit higher orbit precision in all directions than the BDS satellites because of much better observation geometry. The RMS in the along-track and cross-track directions is comparable for each satellite, which is much smaller than that in the

radial direction. When the constraints of predicted satellite clocks are imposed, the average RMS in all directions is reduced, especially in the radial direction where the RMS is reduced by a factor of 7–11, with the value of 9.7 cm and 13.4 cm for GPS and BDS satellites. Equipped with Cs clocks, the G08 and G24 satellites exhibit obviously larger RMS in the radial direction than the other GPS satellites.
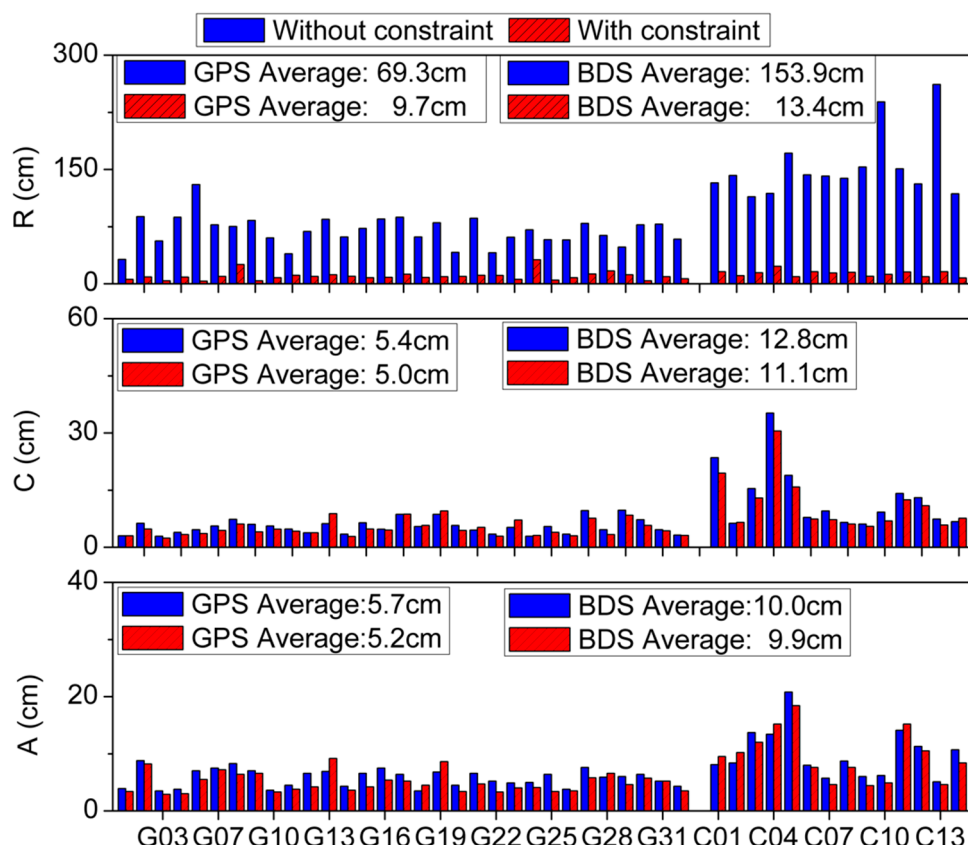
Table 1. Dynamic models and observation models used in the GPS/BDS POD processing.

Item	Applied Models
Geopotential	EGM 2008 model (12 × 12)
M-body gravity	Sun, Moon and planets
Tidal forces	Solid Earth, pole, ocean tide IERS conventions 2010 [32]
Solar Radiation Pressure	Reduced CODE 5-parameter with no initial value
Relativistic effects	IERS conventions 2010
Basic observables	Un-differenced ionosphere-free combinations of code and phase observations on GPS L1/L2, BDS B1/B2
Processing interval	30 s
Cutoff elevation	7°
Weighting	$p = \begin{cases} 1, & e > 30^\circ \\ \sin^2 e, & e \le 30^\circ \end{cases}$
Satellite antenna PCO and PCV	igs08.atx
Receiver antenna PCO and PCV	GPS: igs08.atx BDS: using the same as GPS
Phase wind-up	Corrected [33]
Tropospheric delay	Saastamoinen model (1972) + random-walk process
Satellite clock	Estimated as white noise
Receiver clock	Estimated as white noise
Earth rotation parameters (ERP)	Estimated with tight constraint
Inter-system biases	Estimated as constant parameters
Ambiguity	Fixed for GPS/BDS (IGSO, MEO) separately

Like the standard PPP, the precision of the RPPP POD method depends on the orbital dilution of precision (DOP) that reflects the observation geometry [9]. The DOP in the radial direction is donated as the RDOP and the HDOP represents the DOP in the plane orthogonal to the radial direction, which includes the along-track and cross-track directions. Table 2 lists the HDOP and RDOP for different satellites. Only two GPS satellites are listed as representative, because other GPS satellites have the similar DOP values. It can be seen that the HDOP is significantly smaller than the RDOP, which is consistent with the fact that the orbit accuracy in the along-track and cross-track directions is much better than in the radial direction, as shown in Figure 4. The DOPs of BDS satellites are larger than that of GPS satellites resulting in a much lower orbit accuracy of BDS as well.

Figure 5 illustrates the orbit differences of the two solutions in the along-track, cross-track and radial directions from 22:00:00 to 24:00:00, DOY 124, 2017. As shown in this figure, the RPPP POD solution without clock-constraint exhibits dramatically larger orbit differences in the radial direction than the solution with the clock-constraint, while in the along-track and cross-track directions, both solutions have similar orbit differences whether the clock-constraint is imposed or not. Thus, a clock-constraint in RPPP POD can bring the orbit solution significant improvement in the radial direction but a few improvements in the along-track and cross-track directions. It is noticed that the orbit differences of the unconstrained solution increase slightly with the processing time in all directions.
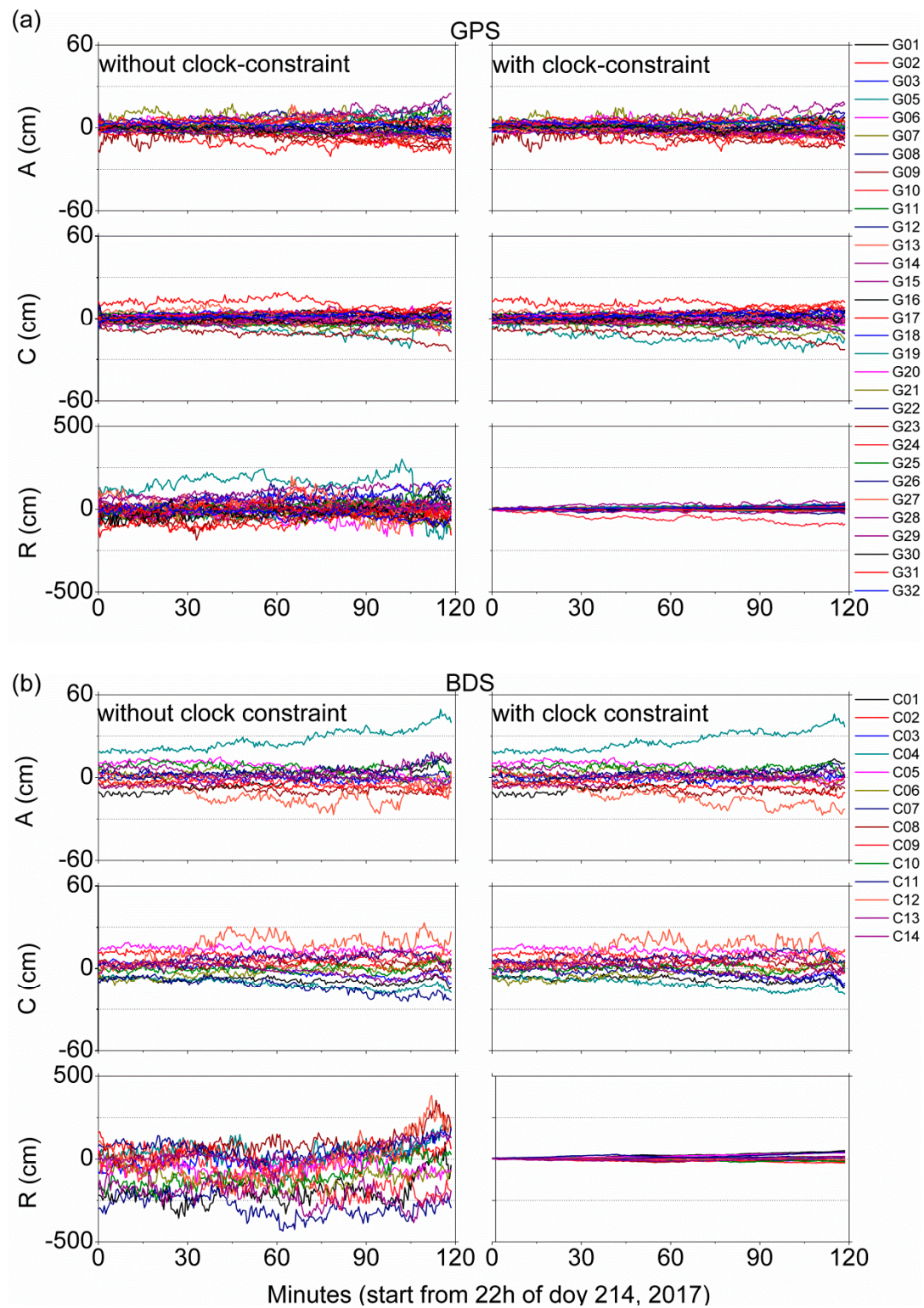
It might because that more cycle slips will occur with the progress of POD processing and the ambiguity parameters consequently increase with processing time, which worsens the estimation of satellite positions. Though significantly reduced, the orbit differences of clock-constrained solutions exhibit more apparent growth rate in the radial direction, which can be attributed to precision degradation of the predicted satellite clocks with processing time.

Figure 4. RMS of GPS and BDS orbit differences in the radial, cross-track and along-track directions of the clock-constrained and traditional RPPP POD solutions with respect to the dynamic POD solution.

Table 2. Orbital dilution of precision (DOPs) for BDS and GPS satellites at 22:00:00, DOY 124, 2017. GEO—geostationary orbit; IGSO—inclined geosynchronous orbit; MEO—Median Earth orbit.

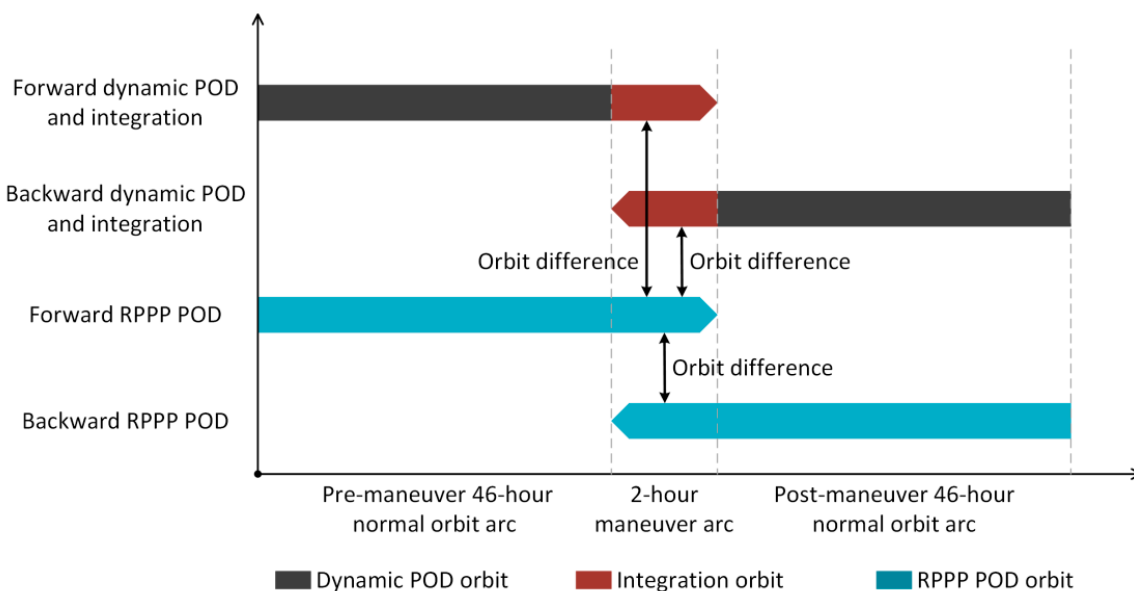| Satellite PRN	Orbit Type	HDOP	RDOP	Number of Stations
C01		3.53	71.07	41
C02		3.96	70.84	28
C03	GEO	3.81	66.28	39
C04		4.28	64.56	34
C05		3.84	69.66	34
C06		3.05	54.78	39
C07		3.38	52.72	41
C08	IGSO	3.31	50.68	39
C09		3.51	73.90	35
C10		3.18	45.69	41
C13		3.79	66.60	33
C11		3.19	28.40	29
C12		3.46	36.68	16
C14	MEO	2.42	27.10	39
G01		2.29	25.29	38
G02		2.37	21.28	37

Figure 5. Orbit differences between the RPPP and dynamic POD solutions for GPS and BDS satellites ((**a**): Orbit differences for GPS satellites; (**b**): Orbit differences for BDS satellites; **left**: RPPP without clock-constraint, **right**: RPPP with clock-constraint).

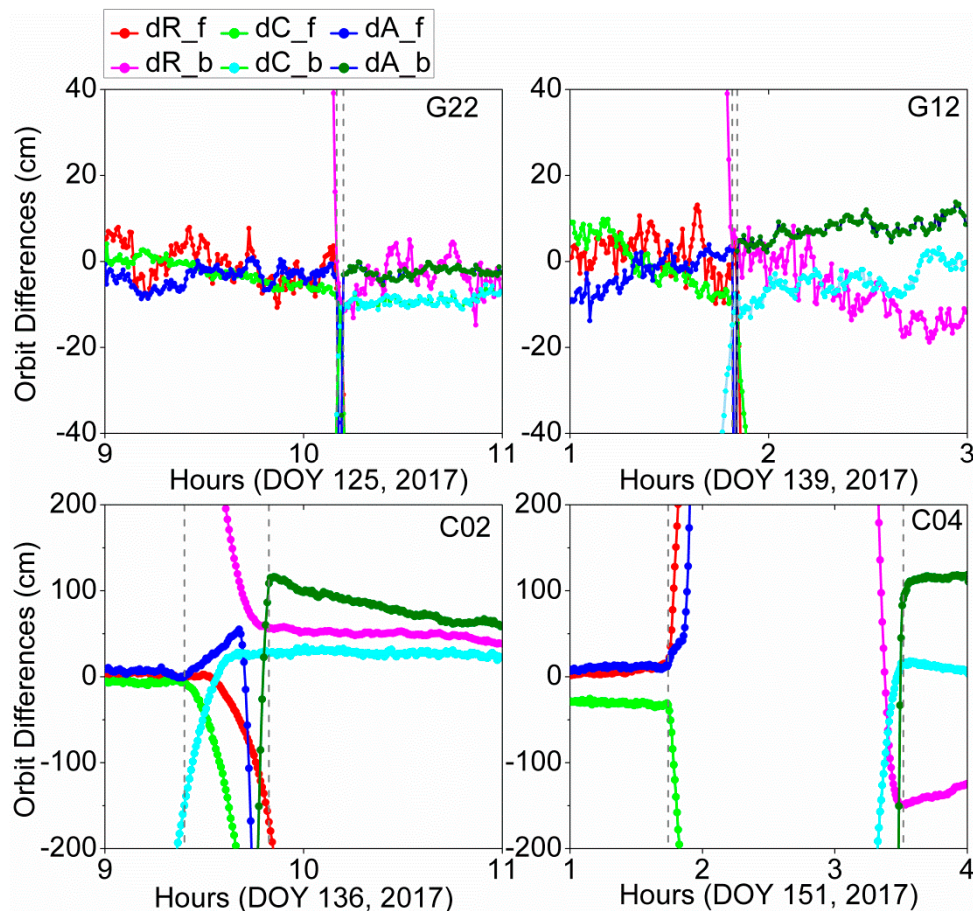### 3.3. Test on the Real Maneuver Cases

The proposed method is further validated by the actual maneuver cases of GPS and BDS satellites. Figure 6 illustrates the POD processing scheme for the maneuvering satellites. As shown in this

figure, after the maneuver time is roughly detected using the method proposed by Qiao et al. [9], we divide the whole 48-h orbit arc into two parts: the normal orbit arc without maneuvers and the 2-h maneuvering orbit arc covering the whole maneuver events. The dynamic POD method is employed with the last 2-h observations of maneuvering satellites excluded to generate precise receiver positions, receiver clocks, ZTDs, ambiguities and IFBs. Then, the clock-constrained RPPP is carried out for the maneuvering satellites within the last 2 h. Since the reference orbits are not available during maneuvering, to evaluate the orbit precision during the maneuvering periods, the clock-constrained RPPP solution is compared with the forward and backward integration orbits based on the dynamic POD estimation before and after maneuvering, respectively. Furthermore, the forward and backward RPPP POD solutions are also compared to validate the accuracy of this method.

Figure 6. Computation and comparison strategy for the maneuvering satellites.

Figure 7 shows the orbit differences between the clock-constrained RPPP solution and the forward and backward integration orbits in the radial, cross-track and along-track directions for G12, G22, C02 and C04 satellites. It is necessary to mention that, the C04 satellites experiences another maneuver about 25 h later after the illustrated one. Thus, the backward POD arc of C04 is set to 24 h to avoid the maneuvering observations, which degrades the dynamic POD precision heavily and introduces significant biases in the orbit differences [34]. Additionally, the C04 maneuver period is a little longer than the others, so we set the maneuver processing arc to 3 h to include the whole maneuver event. The vertical dashed lines indicate the detected start and end time of maneuver events. As shown in this figure, the orbit differences of GPS satellites are less than 20 cm in all the three directions during the normal orbit arcs, which increase rapidly when the satellites are experiencing maneuvers. The extreme enlargements in GPS orbit differences during maneuvering periods can be attributed to the un-modeled maneuver thrust in the dynamic orbit integration. Similarly, the orbit differences of BDS satellites during the normal orbit arcs are less than 30 cm in the radial and cross-track directions and less than 150 cm in the along-track direction, which are much smaller than those during maneuvering periods. Furthermore, because the BDS dynamic models are not as accurate as that of GPS, the fixed parameters in RPPP processing, which are estimated from the dynamic POD before maneuvers, are not well consistent with the parameters estimated from the backward integration orbits, resulting in the discrepancy in the orbit differences before and after maneuvering. We can find that the BDS orbit differences experience three stages during maneuvering periods: gradual changes at the beginning and end stages and rapid changes at the middle stages, which have not been found in GPS orbit differences. In addition, the duration of orbit maneuver for GPS satellites is much shorter than BDS satellites.

Figure 7. Orbit differences between the RPPP solutions and the forward and backward integration orbits for G22, G12, C02 and C04 around maneuvers. The vertical dashed lines indicate the detected start and end time of maneuver events.
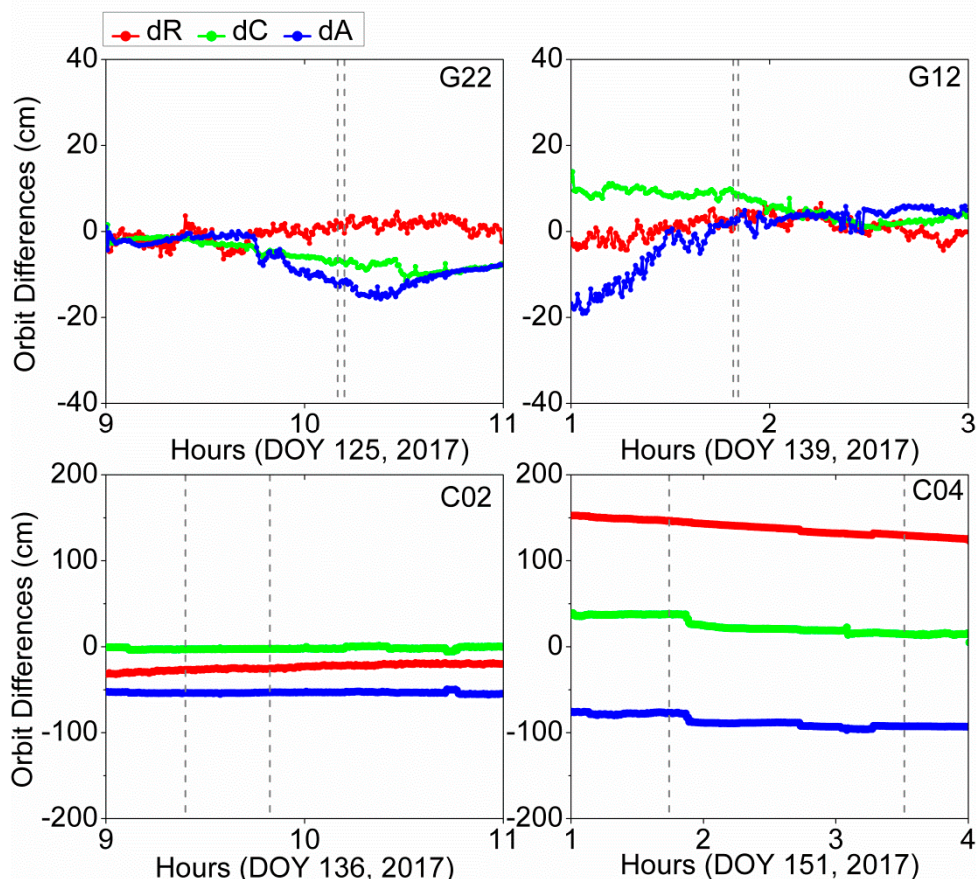
Table 3 presents the detected maneuver time and the unhealthy epochs in broadcast ephemeris for all maneuvering satellites during the experiment period. The maneuver duration of GPS satellites is less than 2 min, while that of BDS satellites is much longer, lasting from 22.5 min to 107 min. The unhealthy periods in the broadcast ephemeris are much longer than the actual maneuver periods when the thrust is applied. It is noticeable that the unhealthy epoch in broadcast ephemeris of G12 is later than the actual maneuver time, which may mislead real-time users and degrade the positioning results.

Table 3. Unhealthy epochs in broadcast ephemeris and detected maneuver time (May in 2017).

PRN	DOY	Unhealthy Epochs in BRDC		Detected Maneuver Time	
		Start and End Time	**Duration**	**Start and End Time**	**Duration**
G22	125	09:59:44–14:00:00	2 h 0 min 16 s	10:11:00–10:12:30	1.5 min
G12	139	01:59:44–07:57:36	5h 57min 52 s	01:50:00–0cd 1:51:00	1 min
C02	136	09:00:00–16:00:00	7 h	09:24:00–09:49:30	25.5 min
C03	139	07:00:00–15:00:00	8 h	08:10:30–08:49:00	38.5 min
C01	142	03:00:00–10:00:00	7 h	05:18:00–05:54:00	36 min
C05	144	23:00:00–05:00:00 (+1d)	6 h	00:29:00 (+1d)–00:51:30	22.5 min
C04	151	01:00:00–09:00:00	8 h	01:44:30–03:31:30	107 min

We further investigated the proposed method by comparing the forward and backward clock-constrained RPPP POD solutions, of which the orbit differences in the radial, cross-track and along-track directions are plotted in Figure 8. As shown in this figure, the orbit differences of

GPS satellites vary in the range of −20 cm to 20 cm in all directions, even in the maneuvering periods. The orbit differences of BDS satellites exhibit similar small variation but obvious bias in all directions. The fixed parameters in the maneuver POD arc in the forward and backward clock-constrained RPPP POD processing are generated from different dynamic POD arcs. Precise force models and good geometric conditions, such as GPS, contribute to precise and consistent parameter estimation and therefore consistent POD solutions for the forward and backward clock-constrained RPPP. Otherwise, the forward RPPP POD solution will be inconsistent with the backward RPPP POD solution, resulting in biases in the orbit differences, such as BDS. The biases of C04 orbit differences are much larger than that of C02, which can be attributed to the short POD arc in the backward processing as mentioned before.

Figure 8. Orbit differences between the forward and backward RPPP solutions for G22, G12, C02 and C04 around maneuvers.

4. Discussion

Maneuver is inevitable for a satellite in space because of various perturbations. Since the precise orbit is unlikely to be determined, a GNSS satellite experiencing maneuvering is useless or even harmful for real-time users if no early warning is provided. The proposed strategy takes the advantage of the fact that GNSS satellites are all equipped with high-precision atomic clocks that are stable in short time and unaffected by maneuvers. The clock offset of a satellite experiencing maneuvering can be precisely predicted based on the clock estimates during the periods before maneuvering, which can provide useful a priori information. With the constraint of predicted clocks, the traditional RPPP POD method has been significantly improved, which contributes to the rather precise orbit for the maneuvering satellites, especially in the radial direction. As the experimental results have shown, the average RMS of clock-constrained RPPP POD solution is dramatically reduced by a factor of 7–11 in the radial direction, which is of great significance to the real-time positioning users.

5. Conclusions

The clock-constrained RPPP method is proposed for POD of GNSS satellites undertaking maneuvers, in which the precise clock estimates from the dynamic POD processing before maneuvering are modeled and predicted to the maneuvering periods to impose a constraint on the satellite clock parameters in RPPP POD during maneuvers. This method depends on the precision of predicted satellite clocks. Thus, the clock prediction models are first developed according to different clock types. The comparison of predicted clocks and GBM final clock products shows that the 2-h prediction error is 0.31 ns and 1.07 ns for GPS Rb and Cs clocks, and 0.45 ns and 0.60 ns for BDS GEO and BDS IGSO/MEO clocks, respectively. This accuracy is sufficient to support the implementation of the proposed method since the duration of maneuver events is usually much less than 2 h.

The proposed method is implemented in the PANDA software and tested on real data. Since the precise orbit products during maneuvering periods are not available, we first evaluate the POD performance of this method with the non-maneuvering data by assuming a satellite experiences orbit maneuvers during the last 2 h of the POD arc. The comparison with dynamic POD solution shows that the accuracy of the unconstrained RPPP POD solution is 69.3 cm, 5.4 cm and 5.7 cm in the radial, cross-track and along-track directions for GPS satellites, and 153.9 cm, 12.8 cm and 10.0 cm for BDS satellites, respectively. When the satellite clock parameters are constrained with the predicted clocks, the average RMS of clock-constrained RPPP POD solution is dramatically reduced in the radial direction by a factor of 7–11, with the value of 9.7 cm and 13.4 cm for GPS and BDS satellites. Then the proposed method is further tested on seven actual maneuver cases, including two GPS maneuver events and five BDS maneuver events in the experiment period. The clock-constrained RPPP POD solution is compared with the forward and backward integration orbits that are calculated from the respective dynamic POD solutions before and after maneuvering. The orbit differences between the clock-constrained RPPP POD solution and the forward and backward integration orbits are less than 20 cm in all three directions for GPS satellite, and less than 30 cm in the radial and cross-track directions and up to 100 cm in the along-track direction for BDS satellites. The maneuver start and end time is detected from the orbit differences, which reveals that the maneuver duration of GPS satellites is less than 2 min, and the maneuver activities last from 22.5 min to 107 min for different BDS satellites.

Author Contributions: Conceptualization, X.D. and Y.L.; methodology, X.D. and Z.D.; software, X.D. and Y.P.; validation, C.S. and Y.L.; formal analysis, X.D.; investigation, C.H., J.Q.; resources, X.D. and C.H.; data curation, X.D. and J.Q.; writing—original draft preparation, X.D., Z.D.; writing—review and editing, Y.L., C.S.; visualization, X.D. and Y.P.; supervision, Y.L. and C.S.; project administration, X.D.; funding acquisition, Y.L. and X.D.

Conflicts of Interest: The authors declare no conflict of interest.

References

1. Kelecy, T.; Hall, D.; Hamada, K.; Stocker, M. Satellite Maneuver Detection Using Two-Line Element (TLE) Data. In Proceedings of the Advanced MAUI Optical and Space Surveillance Technologies Conference, Maui, HI, USA, 12–15 September 2007; pp. 166–181.

2. Song, W.; Wang, R.; Wang, J. A simple and valid analysis method for orbit anomaly detection. *Adv. Space Res.* **2012**, *49*, 386–391. [CrossRef]

3. Hugentobler, U.; Ploner, M.; Schildnecht, T.; Beutler, G. Determina- tion of resonant geopotential terms using optical observations of geostationary satellites. *Adv. Space Res.* **1999**, *23*, 767–770. [CrossRef]

4. Dach, R.; Brockmann, E.; Schaer, S.; Beutler, G.; Meindl, M.; Prange, L.; Bock, H.; Jäggi, A.; Ostini, L. GNSS processing at CODE: Status report. *J. Geod.* **2009**, *83*, 353–366. [CrossRef]

5. Prange, L.; Orliac, E.; Dach, R.; Arnold, D.; Beutler, G.; Schaer, S.; Jäggi, A. CODE's five-system orbit and clock solution—The challenges of multi-GNSS data analysis. *J. Geod.* **2016**, 1–16. [CrossRef]

6.   Xie, J.; Wang, J.; Mi, H. Analysis of Beidou Navigation Satellites In-Orbit State. In *Proceedings of the China Satellite Navigation Conference (CSNC)*; Sun, J., Liu, J., Yang, Y., Fan, S., Eds.; Springer: Berlin, Germany, 2012; pp. 111–122. [CrossRef]

7.   Huang, G.; Qin, Z.; Wang, L.; Yan, X.; Wang, X. An optimized method to detect BDS satellites' orbit maneuvering and anomalies in real-time. *Sensors* **2018**, *18*, 726. [CrossRef]

8.   Hugentobler, U.; Meindl, M.; Beutler, G.; Bock, H.; Dach, R.; Jäggi, A.; Brockmann, E. *CODE IGS Analysis Center Technical Report 2003/2004*; IGS 2004 Technical Reports; Gowey, K., Neilan, R., Moore, A., Eds.; IGS Central Bureau, Jet Propulsion Laboratory: Pasadena, CA, USA, 2006. (in press)

9.   Qiao, J.; Chen, W. Beidou satellite maneuver thrust force estimation for precise orbit determination. *GPS Solut.* **2018**, *22*, 42. [CrossRef]

10.   Yan, X.; Huang, G.; Zhang, R.; Zhang, Q. A method based on broadcast ephemeris to detect BDS satellite orbital maneuver. *J. Navig. Position* **2015**, *3*, 35–38.

11.   Ye, F.; Yuan, Y.; Tan, B.; Ou, J. A robust method to detect BeiDou navigation satellite system orbit maneuvering/anomalies and its applications to precise orbit determination. *Sensors* **2017**, *17*, 1129. [CrossRef]

12.   Huang, G.; Qin, Z.; Zhang, Q.; Wang, L.; Yan, X.; Fan, L.; Wang, X. A real-time robust method to detect BeiDou GEO/IGSO orbital maneuvers. *Sensors* **2017**, *17*, 2761. [CrossRef]

13.   Jäggi, A.; Montenbruck, O.; Moon, Y.; Wermuth, M.; König, R.; Michalak, G.; Bock, H.; Bodenmann, D. Inter-agency comparison of TanDEM-X baseline solutions. *Adv. Space Res.* **2012**, *50*, 260–271. [CrossRef]

14.   Ju, B.; Gu, D.; Herring, T.A.; Allende-Alba, G.; Montenbruck, O.; Wang, Z. Precise orbit and baseline determination for maneu- vering low earth orbiters. *GPS Solut.* **2017**, *21*, 53–64. [CrossRef]

15.   Beutler, G.; Jäggi, A.; Hugentobler, U.; Mervart, L. Efficient satellite orbit modelling using pseudo-stochastic parameters. *J. Geod.* **2006**, *80*, 353–372. [CrossRef]

16.   Song, X.; Mao, Y.; Ren, K.; Jia, X. Comparing the applicability of two kinds of thrust model for maneuver orbit. *Geomat. Inf. Sci. Wuhan Univ.* **2013**, *38*, 1196–1200.

17.   Cao, F.; Yang, X.; Li, Z.; Sun, B.; Kong, Y.; Chen, L.; Feng, C. Orbit determination and prediction of GEO satellite of BeiDou during repositioning maneuver. *Adv. Space Res.* **2014**, *54*, 1828. [CrossRef]

18.   Zhou, P.; Du, L.; Li, X.; Gao, Y. Near real-time BDS GEO satellite orbit determination and maneuver analysis with reversed point positioning. *Adv. Space Res.* **2018**, *63*, 1781–1791. [CrossRef]

19.   Guo, R.; Zhou, J.; Hu, X.; Liu, L.; Tang, B.; Li, X.; Sun, S. Precise orbit determination and rapid orbit recovery supported by time synchronization. *Adv. Space Res.* **2015**, *55*, 2889. [CrossRef]

20.   Huang, G.; Zhang, Q.; Xu, G. Real-time clock offset prediction with an improved model. *GPS Solut.* **2014**, *18*, 95–104. [CrossRef]

21.   Heo, Y.; Cho, J.; Heo, M. Improving prediction accuracy of GPS satellite clocks with periodic variation behaviour. *Meas. Sci. Technol.* **2010**, *21*, 073001. [CrossRef]

22.   Shmaliy, Y.; Marienko, A.; Savchuk, A. GPS-Based Optimal Kalman Estimation of Time Error, Frequency Offset, and Aging. In Proceedings of the 31st Annual Precise Time and Time Interval Meeting, Dana Point, CA, USA, 7–9 December 1999; pp. 431–440.

23.   Senior, K.; Ray, J.; Beard, R. Characterization of periodic variations in the GPS satellite clocks. *GPS Solut.* **2008**, *12*, 211–225. [CrossRef]

24.   Nie, Z.; Gao, Y.; Wang, Z.; Ji, S.; Yang, H. An approach to GPS clock prediction for real-time PPP during outages of RTS stream. *GPS Solut.* **2018**, *22*, 14. [CrossRef]

25.   Uhlemann, M.; Gendt, G.; Ramatschi, M.; Deng, Z. *GFZ Global Multi-GNSS Network and Data Processing Results*; Springer: Cham, Switzerland, 2015; pp. 673–679.

26.   Huang, G.; Zhang, Q. Real-time estimation of satellite clock offset using adaptively robust Kalman filter with classified adaptive factors. *GPS Solut.* **2012**, *16*, 531–539. [CrossRef]

27.   Dow, J.M.; Neilan, R.E.; Rizos, C. The International GNSS Service in a changing landscape of Global Navigation Satellite Systems. *J. Geod.* **2009**, *83*, 191–198. [CrossRef]

28.   Montenbruck, O.; Steigenberger, P.; Prange, L.; Deng, Z.; Zhao, Q.; Perosanz, F.; Schmid, R. The Multi-GNSS Experiment (MGEX) of the International GNSS Service (IGS)—achievements, prospects and challenges. *Adv. Space Res.* **2017**, *59*, 1671. [CrossRef]

29.   Liu, J.; Ge, M. PANDA software and its preliminary result of positioning and orbit determination. *Wuhan Univ. J. Nat. Sci.* **2003**, *8*, 603–609. [CrossRef]

30. Shi, C.; Zhao, Q.; Geng, J.; Lou, Y.; Ge, M.; Liu, J. Recent Development of PANDA Software in GNSS Data Processing. *Proc. Spie.* **2008**, *7285*, 231–249. [CrossRef]

31. Springer, T.; Beutler, G.; Rothacher, M. Improving the orbit estimates of GPS satellites. *J. Geod.* **1999**, *73*, 147–157. [CrossRef]

32. Petit, G.; Luzum, B. *IERS Conventions 2010*; Iers Technical Note 36; Verlag des Bundesamts für Kartographie und Geodäsie: Frankfurt am Main, German, 2010; Volume 36, pp. 1–95. ISBN 3-89888-989-6.

33. Wu, J.T.; Wu, S.C.; Hajj, G.A.; Bertiger, W.I.; Lichten, S.M. Effects of antenna orientation on GPS carrier phase. *Manuscr. Geod.* **1993**, *18*, 91–98.

34. Geng, T.; Zhang, P.; Wang, W.; Xie, X. Comparison of Ultra-Rapid Orbit Prediction Strategies for GPS, GLONASS, Galileo and BeiDou. *Sensors* **2018**, *18*, 477. [CrossRef]